ResearchGate

See discussions, stats, and author profiles for this publication at: https://www.researchgate.net/publication/232736524

Electrostatic Spray Deposition of Porous SnO2/Graphene Anode Films and Their Enhanced Lithium-Storage Properties

ARTICLE *in* ACS APPLIED MATERIALS & INTERFACES · OCTOBER 2012

Impact Factor: 6.72 · DOI: 10.1021/am301788m · Source: PubMed

CITATIONS
27

READS
105

4 AUTHORS, INCLUDING:

Yinzhu Jiang
Zhejiang University
60 PUBLICATIONS **636** CITATIONS
SEE PROFILE

Tianzhi Yuan
Zhejiang University
8 PUBLICATIONS **109** CITATIONS
SEE PROFILE

Wenping Sun
Institute for Superconducting & Electronic Mat…
73 PUBLICATIONS **811** CITATIONS
SEE PROFILE

Available from: Wenping Sun
Retrieved on: 24 January 2016

ACS APPLIED MATERIALS & INTERFACES

Research Article

www.acsami.org

Electrostatic Spray Deposition of Porous SnO_2/Graphene Anode Films and Their Enhanced Lithium-Storage Properties

Yinzhu Jiang,*[,†] Tianzhi Yuan,[†] Wenping Sun,[‡] and Mi Yan*[,†]

[†] State Key Laboratory of Silicon Materials, Key Laboratory of Advanced Materials and Applications for Batteries of Zhejiang Province, Department of Materials Science and Engineering, Zhejiang University, Hangzhou 310027, China

[‡] CAS Key Laboratory of Materials for Energy Conversion, Department of Materials Science and Engineering, University of Science and Technology of China (USTC), Hefei, 230026, China

ABSTRACT: Porous SnO_2/graphene composite thin films are prepared as anodes for lithium ion batteries by the electrostatic spray deposition technique. Reticular-structured SnO_2 is formed on both the nickel foam substrate and the surface of graphene sheets according to the scanning electron microscopy (SEM) results. Such an assembly mode of graphene and SnO_2 is highly beneficial to the electrochemical performance improvement by increasing the electrical conductivity and releasing the volume change of the anode. The novel engineered anode possesses 2134.3 mA h g^{-1} of initial discharge capacity and good capacity retention of 551.0 mA h g^{-1} up to the 100th cycle at a current density of 200 mA g^{-1}. This anode also exhibits excellent rate capability, with a reversible capacity of 507.7 mA h g^{-1} after 100 cycles at a current density of 800 mA g^{-1}. The results demonstrate that such a film-type hybrid anode shows great potential for application in high-energy lithium-ion batteries.

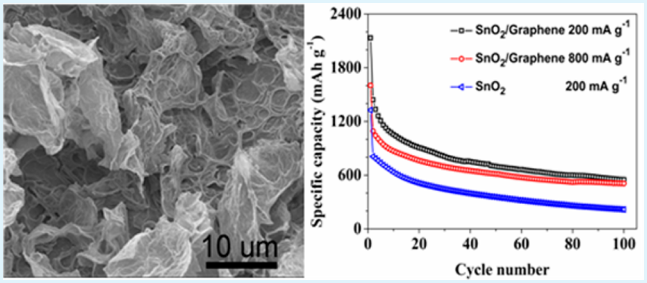

KEYWORDS: *electrochemical spray deposition, tin oxide, graphene, thin films, lithium ion battery*

INTRODUCTION

Lithium-ion batteries (LIBs) are currently the dominant power sources for portable electronic devices, and have been regarded as the most promising power sources for electric/hybrid vehicles. The anode is one of the most important components in a LIB since the overall performance is largely determined by its capability of absorbing/desorbing lithium ions. Graphite is the-state-of-art anode material for commercial LIBs, but its limited specific capacity (theoretically 372 mA h g^{-1}) cannot satisfy the increasing demand for batteries with higher energy density.[1] In the past decade, a lot of efforts were made to explore alternative anode materials with higher lithium storage capacity. Among these materials, tin oxide has attracted much attention because of its high theoretical reversible capacity (e.g., 781 mA h g^{-1} for SnO_2), nontoxicity and good processability. However, the volume change of tin oxide is enormous (up to 259%) during discharge/charge cycle, and the volume change will result in mechanical failure, electrical disconnection, and capacity loss of the anode. Therefore, tin oxide-based anode cannot meet the strict demands of practical applications if no microstructure or composition improvement is made.[2−4]

To mitigate the negative effects of the volume change, two strategies have been proposed. One is to design tin oxide anode with various structures such as hollow, porous, core−shell, and nanowires,[5−8] the other one is to hybridize tin oxide with carbonaceous materials.[9,10] In recent years, graphene, as the basis plane of graphite, has attracted considerable interest since it was first reported by Novoselov et al..[11] Graphene has high surface area, large surface-to-volume ratio, superior electronic conductivity and high mechanical strength.[12,13] Hence, graphene appears to be an ideal material for hybridizing with SnO_2 to improve the capacity and cycling stability of the anode. Up till now, there have been a few reports about the preparation of SnO_2/graphene composite.[4,14−16] However, it should be noted that all the reported works are focused on synthesizing composite powders, which still need to be mixed with conductive additives and binders for fabricating the anode. The processes of mixing and grinding may alter the morphology of the as-synthesized powders as well as decrease the effective loading of the active materials.

Here, we fabricated porous SnO_2/graphene composite films by the electrostatic spray deposition (ESD) technique for the first time, and the film-type composite was investigated as the anode of LIBs directly without extra binder and conductive matters. The crystal structure, surface morphology, and electrochemical performances of the SnO_2/graphene composite anodes were investigated. It is expected that the combined effect, of such highly porous hybrid material would mitigate the volume change effect, and then exhibit enhanced specific capacity and cycling stability.

Received: August 29, 2012
Accepted: October 29, 2012
Published: October 29, 2012

 © 2012 American Chemical Society

EXPERIMENTAL SECTION

Preparation of SnO_2/Graphene Film. Porous SnO_2/graphene thin films were prepared by the ESD technique, which is similar to that described in the literature.[17] All films were deposited on nickel foam substrates kept at 200 °C. The distance and DC voltage between the nozzle and substrate was 4 cm and 15−16 kV, respectively. The precursor solution of 0.005 M $Sn(NO_3)_2$ with a solvent composed of 40% ethanol +40% 1,2-propanediol +20% glycol, which was used for depositing pure SnO_2 anode film, were obtained through the stoichiometric reaction between $SnCl_2$ and $AgNO_3$. To fabricate SnO_2/graphene composite, 3.8 mg of chemical reduced graphene powder was added into 50 mL of 0.005 M $Sn(NO_3)_2$ solution described above first. The suspension was then homogenized using a high power ultrasonic dispenser for 10 min at 60% of maximum amplitude. The resultant precursor suspension was pumped at 2 mL h^{-1} into a stainless steel nozzle (inner diameter, 0.8 mm) for the deposition of SnO_2/graphene anode film. The mass of the deposited material was measured using a microbalance with an accuracy of 0.002 mg (Sartorius CPA26P, Germany) before and after deposition.

Materials Characterization. The crystal structures of the graphene powders and SnO_2/graphene thin films were identified by X-ray diffraction (XRD) on a Rigaku D/Max-2550pc diffractometer equipped with Cu K_α radiation (λ = 1.5406 Å), with a scan range of 10−80°. The surface morphology was characterized by scanning electron microscopy (SEM, Hitachi S-4800). The Raman spectrum was recorded on a Renishaw inVia Raman Microscope (532 nm).

Electrochemical Measurements. The electrochemical behavior was examined in CR2025 coin-type cells using the as-deposited films on nickel foam as the working electrode and lithium foil as the counter and reference electrode, respectively. Cell assemble was carried out in an argon filled glovebox, in which the oxygen concentration and moisture level were maintained less than 1 ppm. Celgard 2300 microporous polypropylene was used as a separator. The electrolyte was 1 M $LiPF_6$ in ethylene carbonate (EC)/dimethyl carbonate (DMC) (1:1 by volume). The cells were charged and discharged galvanostatically on a Neware BTS-5 V1 mA battery cycler at 0.01−3 V (vs Li/Li^+). Cyclic voltammetry (CV) tests were conducted on a CHI660C electrochemistry workstation between 0.01 and 3.0 V (vs Li/Li^+) at 0.1 mV s^{-1}. All the electrochemical measurements were carried out at room temperature.

RESULTS AND DISCUSSION

Figure 1a shows the XRD pattern of the SnO_2/graphene thin film deposited at 200 °C. Except for the diffraction peaks corresponding to the nickel substrate, no other peaks can be discerned. After annealed at 500 °C for 3 h in high purity Ar atmosphere, two new broad and weak peaks at 26.6 and 33.9° appear in the XRD pattern (Figure 1b), which can be assigned to the (110) and (101) planes of SnO_2 (JCPDS Card No. 41−1445), respectively. The results indicate that the deposition temperature of 200 °C is too low for the crystallization of SnO_2 and hence the as-deposited film is amorphous. The inset of Figure 1 shows the XRD pattern of the pure graphene powders, which clearly reveals the typical characteristic of graphene with a strong (002) diffraction peak and a weak (100) diffraction one. However, no diffraction peak assigned to graphene is found in the pattern of the composite, because the strong diffraction signals of nickel foam sheltered the typical characteristics of small amount graphene sheets.[18]

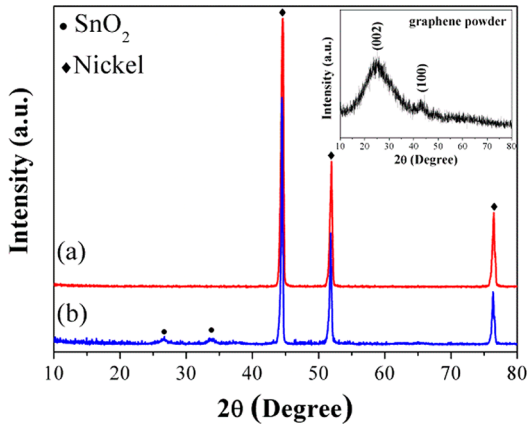

Figure 1. X-ray diffraction patterns of (a) the as-deposited SnO_2/graphene thin film, and (b) the SnO_2/graphene thin film annealed at 500 °C. The inset shows the XRD pattern of graphene powders.

Raman spectroscopy is a powerful tool to investigate graphene sheets in the composite. As seen from Figure 2, the

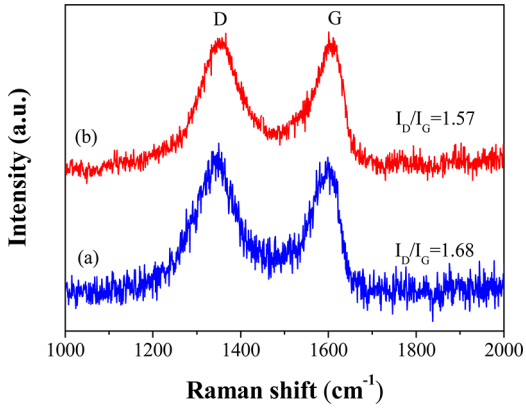

Figure 2. Raman spectrum of (a) the pure graphene powders and (b) the SnO_2/graphene thin film.

Raman spectrum of the pure graphene powders contains both G band (~1593 cm^{-1}, E_{2g} phonon of sp^2 atoms) and D bands (~1358 cm^{-1}, *k*-point phonons of A_{1g} symmetry).[19] Both G and D bands are also observed in the Raman spectrum of the SnO_2/graphene thin film, which confirms the presence of the graphene in the composite. The intensity ratio of the D to G band (I_D/I_G) was calculated as 1.68 for the pure graphene powders and 1.57 for the SnO_2/graphene composite film. The decreased I_D/I_G ratio of the SnO_2/graphene composite film compared with that of the pure graphene powders may be due to the decreased sample defects created by the attachment of functional groups on the carbon.[20] When graphene sheets were mixed with Sn^{2+} ions, partial of the Sn^{2+} ions were attracted and anchored to these functional groups, which leads to the decrease of the number of oxygen-containing functional groups along with the oxidation of Sn^{2+} to Sn^{4+}.

Figure 3a−d shows surface morphology of the as-deposited pure SnO_2 and SnO_2/graphene thin films taken at different magnifications. As can be seen from Figure 3a, pure SnO_2 film exhibits a reticular three-dimensional porous structure which is similar as the early reported results on ESD-derived materials. The reticular SnO_2 structure has inner holes with diameters up to few micrometers. While incorporated with graphene sheets in the deposition process, it is observed that curled graphene sheets are embedded uniformly into reticular-like porous SnO_2 matrix, as shown in Figure 3b, c. Interestingly, similar reticular structured SnO_2 was also grown on the surface of graphene sheets, as can be clearly seen in Figure 3d. Such a microstructure of SnO_2 network entangled graphene is obviously different from that of pure graphene powders (Figure

dx.doi.org/10.1021/am301788m | ACS Appl. Mater. Interfaces 2012, 4, 6216−6220

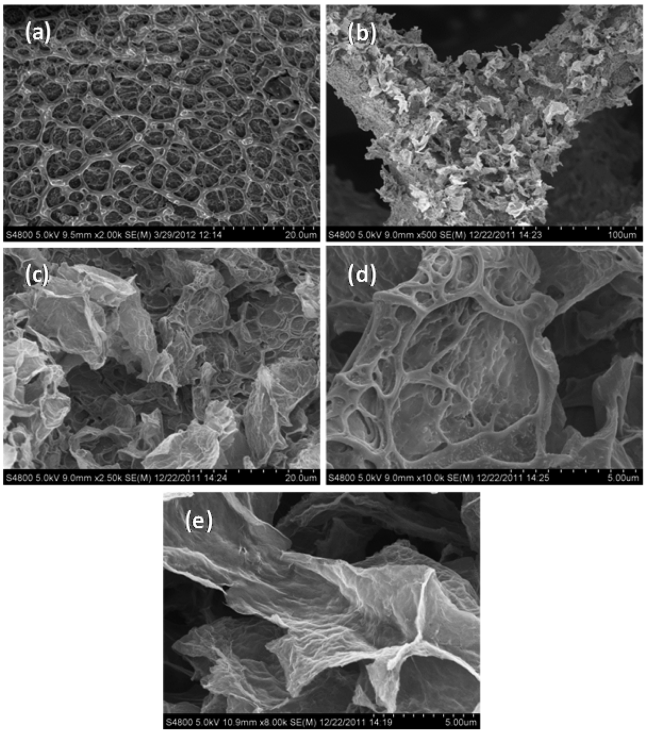

Figure 3. SEM images of (a) the as-deposited pure SnO_2 thin film and (b–d) the as-deposited SnO_2/graphene thin films at different magnifications. (e) SEM images of the pure graphene powders.

3e), indicating a strong interaction between the SnO_2 network and graphene sheets. This unique structure might effectively prevent the peeling of graphene sheets during cycling. In the hybrid film, the graphene sheets act as electronic conductive channels to improve the electrochemical performances, whereas the porous reticular SnO_2 structure could accommodate the volume variation of the anode during the alloying and dealloying processes.

The charge/discharge curves of the cell with the SnO_2/graphene composite film anode were evaluated in the voltage range of 0.01 to 3.0 V (versus Li/Li^+) at a constant current density of 200 mA g^{-1}. The initial two charge/discharge curves are shown in Figure 4a. The first discharge and charge capacity of the cell achieved 2134.3 and 1428.6 mA h g^{-1}, respectively. Currently, practical applications of SnO_2 anode is heavily restricted by its low initial Coulombic efficiency, which results from the formation of the solid-electrolyte interphase (SEI) layer and the irreversible conversion from Sn(IV) to Sn(0).[21] Surprisingly, the initial Coulombic efficiency of the SnO_2/graphene composite film is as high as 66.9%, which is higher than that of the pure SnO_2 film in the present work (60.9%, Figure 4b) and most other reports.[4,22] The improvement of the initial Coulombic efficiency should be attributed to the unique hybrid structure of the SnO_2/graphene thin film. Besides, it can be observed that the first reversible capacity is also much higher than the theoretical capacity, the reason for which will be discussed in the following part.

To investigate the electrochemical reactions in more detail, CV profiles of the cell with the SnO_2/graphene film anode from the first to the third cycle were characterized, as shown in Figure 4c. A sweep rate of 0.1 mV s^{-1} and a voltage range from 0.01 to 3.00 V were employed to investigate the full range of the lithium storage behavior. During the first discharge cycle,

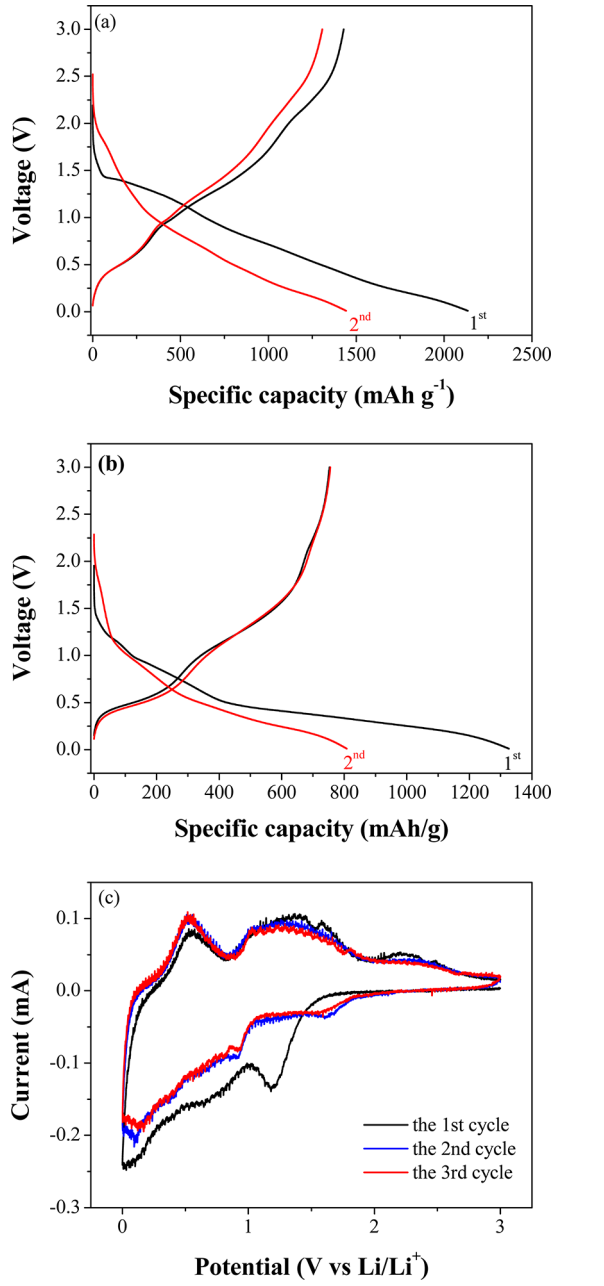

Figure 4. Initial two voltage-capacity curves of (a) the SnO_2/graphene composite film electrode and (b) SnO_2 electrode cycled between 0.01 and 3.0 V versus Li^+/Li at 200 mA g^{-1}. (c) Cyclic voltammograms of the SnO_2/graphene composite film electrode from the first cycle to the third cycle at a scan rate of 0.1 mV s^{-1} between 0.01 and 3 V.

there are three reduction peaks at 1.2 V, 0.5–1.0 V, and ~0.1 V, respectively. The obvious reduction peak centered at 1.2 V should be attributed to the reduction of SnO_2 to SnO and the formation of Li_2O (eq 1), respectively, whereas the broad reduction peak in the range of 0.5–1.0 V corresponds to the conversion of SnO to Sn (eq 2), the conversion of SnO_2 and Li^+ to Sn and Li_2O (eq 3), and the formation of an SEI layer as well.[23] The third reduction peak around 0.1 V reflects Li–Sn alloying and the intercalation of lithium ion into the graphene layers (eqs 4–5).

$$SnO_2 + 2Li^+ + 2e^- \leftrightarrow SnO + Li_2O \quad (1)$$

dx.doi.org/10.1021/am301788m | ACS Appl. Mater. Interfaces 2012, 4, 6216–6220

$$SnO + 2Li^+ + 2e^- \leftrightarrow Sn + Li_2O \quad (2)$$

$$4Li^+ + SnO_2 + 4e^- \rightarrow 2Li_2O + Sn \quad (3)$$

$$xLi^+ + Sn + xe^- \leftrightarrow Li_xSn (0 \le x \le 4.4) \quad (4)$$

$$xLi^+ + C(\text{graphene}) + xe^- \leftrightarrow Li_xC \quad (5)$$

Two oxidation peaks appear around 0.55 and 1.28 V in the first charge cycle curve. The oxidation peak around 0.55 V can be assigned to the dealloying of Li_xSn, whereas the weak oxidation peak at 1.28 V is most likely due to partial reversibility of SnO_2 and SnO to Sn (eqs 1 and 2).[24] In our opinion, the reversibility should mainly contribute to the extra capacity of SnO_2/graphene composite anode compared with the theoretical capacity. Besides, it can be observed that the second and third cycle curves come to coinciding in shape, suggesting that the electrochemical reactions between lithium ions and the SnO_2/graphene anode are reversible. In addition, the Li insertion/extraction on the surface of graphene sheets may also contribute to the excess capacity of the SnO_2/graphene composite anode.[25]

The cycling stability of the SnO_2/graphene composite film anode between 0.01 and 3 V was also studied at a constant current density of 200 mA g^{-1}. The performance of pure SnO_2 thin film electrode was included for comparison. As shown in Figure 5, the discharge capacity drops from 2134.3 to 1442.2 mA h g^{-1} for the SnO_2/graphene composite film anode after the first cycle, whereas it drops from 1326.5 to 808.4 mA h g^{-1} for the pure SnO_2 film anode. Clearly, the SnO_2/graphene thin film exhibits a significantly higher initial capacity than pure SnO_2 film. After 100 charge−discharge cycles, a reversible capacity of 551.0 mA h g^{-1} can be delivered for the porous SnO_2/graphene thin film, corresponding to 38.2% retention of the second discharge capacity and 0.6% capacity drop per cycle. In contrast, the pure SnO_2 film can only deliver a capacity of 217.2 mA h g^{-1}, which is about 26.9% retention of the second discharge capacity. The unique geometric microstructure of the porous SnO_2/graphene thin film anode should be responsible for its significantly improved performance and stability. In comparison with the pure SnO_2 film, reticular SnO_2 structures were grown on both nickel foam and the surface of graphene sheets for the SnO_2/graphene composite film. The special microstructure introduces more contact area between SnO_2 and electrolyte, and hence offers more lithium insertion/extraction sites for higher discharge and charge capacities.[25] At the same time, the firm contact between the porous SnO_2 structure and graphene sheets ensures high capacity and good cycling stability of the porous SnO_2/graphene thin film. As discussed previously, graphene sheets provide a highly conductive medium for electron transfer during the lithiumion insertion/desertion process, and reticular SnO_2 structure offers a "buffer-zone" to accommodate the large volume changes of Sn particles during charging/discharging. To evaluate the rate performance of the SnO_2/graphene film, the charge/discharge measurements were also carried out at a higher current density of 800 mA g^{-1}. It was found that the SnO_2/graphene film was still able to deliver a capacity of 507.7 mA h g^{-1} after 100 cycles. Despite that the charge/discharge capacity of the SnO_2/graphene thin film declines with increasing the current density, the film still shows an excellent cycling performance, further confirming that the hybridization of porous SnO_2 film and graphene is a quite effective strategy to obtain stable high energy lithium ion batteries.

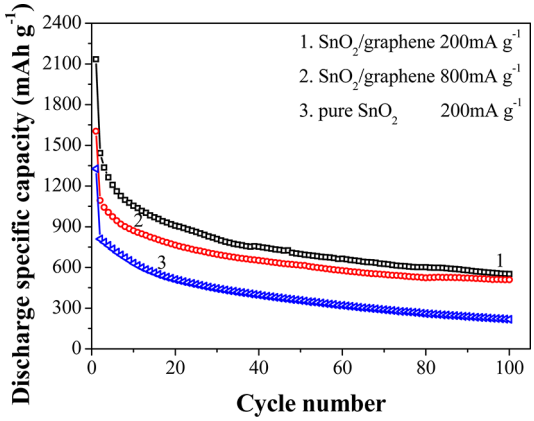

Figure 5. Comparison of cycling performance of the pure SnO_2 film anode at a current density of 200 mA g^{-1} and the SnO_2/graphene composite films at a current density of 200 and 800 mA g^{-1}, respectively between 0.01 and 3.0 V.

CONCLUSION

In summary, porous SnO_2/graphene composite film anode for lithium ion batteries was successfully fabricated using the ESD technique. Compared to the pure SnO_2 thin film, the SnO_2/graphene composite film exhibited much better electrochemical performances and cycling stability. This porous SnO_2/graphene anode possessed a capacity of 2134.3 and 1428.6 mAh g^{-1} for the first discharge and charge cycle, respectively, at a current density of 200 mA g^{-1}; at the same time, showed good capacity retention with a capacity of 551.0 mA h g^{-1} after 100 cycles. The new anode also exhibited excellent rate capability with an 800 mA g^{-1} rate capacity up to 507.7 mA h g^{-1}. The promising electrochemical performances should be attributed to the excellent microstructure of the new anode. Not only the porous reticular microstructure but also the firm contact between SnO_2 and graphene are highly beneficial to obtain high capacity and good cycling stability. The results indicate that the porous SnO_2/graphene composite thin film might be a promising alternative anode for stable high-energy lithium-ion batteries.

AUTHOR INFORMATION

Corresponding Author

*E-mail: yzjiang@zju.edu.cn (Y.J.); mse_yanmi@zju.edu.cn (M.Y.). Tel/Fax: 86-571-87952366 (Y.J.); Tel/Fax: 86-571-87952366 (M.Y.).

Notes

The authors declare no competing financial interest.

ACKNOWLEDGMENTS

This work is supported by National Natural Science Foundation of China (Grant 51102213).

REFERENCES

(1) Dahn, J. R.; Zheng, T.; Liu, Y.; Xue, J. S. *Science* **1995**, *270*, 590.
(2) Fan, J.; Wang, T.; Yu, C.; Tu, B.; Jiang, Z.; Zhao, D. *Adv. Mater.* **2004**, *16*, 1432.
(3) Wang, Y.; Lee, J. Y.; Zeng, H. C. *Chem. Mater.* **2005**, *17*, 3899.
(4) Yao, J.; Shen, X. P.; Wang, B.; Liu, H. K.; Wang, G. X. *Electrochem. Commun.* **2009**, *11*, 1849.
(5) Han, S.; Jang, B.; Kim, T.; Oh, S. M.; Hyeon, T. *Adv. Funct. Mater.* **2005**, *15*, 1845.

(6) Lou, X. W.; Wang, Y.; Yuan, C.; Lee, J. Y.; Archer, L. A. *Adv. Mater.* **2006**, *18*, 2325.
(7) Park, M. S.; Wang, G. X.; Kang, Y. M.; Wexler, D.; Dou, S. X.; Liu, H. K. *Angew. Chem., Int. Ed.* **2007**, *119*, 764.
(8) Yu, Y.; Gu, L.; Dhanabalan, A.; Chen, C. H.; Wang, C. L. *Electrochim. Acta* **2009**, *54*, 7227.
(9) Wang, Y.; Lee, J. Y. *Electrochem. Commun.* **2003**, *5*, 292.
(10) Ren, J.; Yang, J.; Abouimrane, A.; Wang, D.; Amine, K. *J. Power Sources* **2011**, *196*, 8701.
(11) Novoselov, K. S.; Geim, A. K.; Morozov, S. V.; Jiang, D.; Zhang, Y.; Dubonos, S. V.; Grigorieva, I. V.; Firsov, A. A. *Science* **2004**, *306*, 666.
(12) Stankovich, S.; Dikin, D. A.; Dommett, G. H. B.; Kohlhaas, K. M.; Zimney, E. J.; Stach, E. A.; Piner, R. D.; Nguyen, S. T.; Ruoff, R. S. *Nature* **2006**, *442*, 282.
(13) Pumera, M. *Energy Environ. Sci.* **2011**, *4*, 668.
(14) Paek, S. M.; Yoo, E.; Honma, I. *Nano Lett.* **2009**, *9*, 72.
(15) Zhang, M.; Lei, D.; Du, Z. F.; Yin, X. M.; Chen, L. B.; Li, Q. H.; Wang, Y. G.; Wang, T. H. *J. Mater. Chem.* **2011**, *21*, 1673.
(16) Li, X.; Meng, X.; Liu, J.; Geng, D.; Zhang, Y.; Banis, M. N.; Li, Y.; Yang, J.; Li, R.; Sun, X.; Cai, M.; Verbrugge, M. W. *Adv. Funct. Mater.* **2012**, *22*, 1647.
(17) Chen, C. H.; Kelder, E. M.; Schoonman, J. *J. Electrochem. Soc.* **1997**, *144*, L289.
(18) Xia, X. H.; Tu, J. P.; Mai, Y. J.; Chen, R.; Wang, X. L.; Gu, C. D.; Zhao, X. B. *Chem.- -Eur. J.* **2011**, *17*, 10898.
(19) Zhao, B.; Zhang, G.; Song, J.; Jiang, Y.; Zhuang, H.; Liu, P.; Fang, T. *Electrochim. Acta* **2011**, *56*, 7340.
(20) Shao, G. L.; Lu, Y. G.; Wu, F. F.; Yang, C. L.; Zeng, F. L.; Wu, Q. L. *J. Mater. Sci.* **2012**, *47*, 4400.
(21) Kim, M. G.; Cho, J. *Adv. Funct. Mater.* **2009**, *19*, 1497.
(22) Park, K. S.; Kang, J. G.; Choi, Y. J.; Lee, S.; Kim, D. W.; Park, J. G. *Energy Environ. Sci.* **2011**, *4*, 1796.
(23) Ferrara, G.; Damen, L.; Arbizzani, C.; Inguanta, R.; Piazza, S.; Sunseri, C.; Mastragostino, M. *J. Power Sources* **2011**, *196*, 1469.
(24) Luo, B.; Wang, B.; Liang, M.; Ning, J.; Li, X.; Zhi, L. *Adv. Mater.* **2012**, *24*, 1405.
(25) Zhu, X.; Zhu, Y.; Murali, S.; Stoller, M. D.; Ruoff, R. S. *J. Power Sources* **2011**, *196*, 6473.